Spin-wave modes localized on isolated defects in a two-dimensional array of dipolarly coupled magnetic nanodots

R. V. Verba [1,*], E. G. Galkina,[2] V. S. Tiberkevich,[3] A. N. Slavin,[3] and B. A. Ivanov [1,4]

[1]*Institute of Magnetism, Kyiv 03142, Ukraine*
[2]*Institute of Physics, National Academy of Sciences of Ukraine, Kyiv 03028, Ukraine*
[3]*Department of Physics, Oakland University, Rochester, Michigan 48309, USA*
[4]*National University of Science and Technology "MISiS," Moscow 119049, Russian Federation*

A comprehensive analytical and numerical study of spin-wave (SW) modes localized on isolated defects in a two-dimensional array of dipolarly coupled magnetic nanodots is presented. Two limiting cases of a defect dot are considered: (i) pointlike defect—a dot having a different eigenfrequency, but the same magnetic moment; (ii) "dipolar defect"—a dot having a different magnetic moment. It is shown, that the appearance of a localized SW mode depends on the peculiarities of the bulk SW spectrum near its bottom or/and top boundaries. In the case of a smooth parabolic spectrum, a localized mode can be created by a defect of a vanishingly small strength, whereas in the case of a spectrum described by a nonanalytic function a localized mode can be created only by a defect of a finite strength, exceeding a certain threshold value. In contrast to the pointlike defects, the dipolar defects may lead to the formation of higher-order localized SW modes. In a case of a complex array having several spin-wave branches (e.g., an array existing in an antiferromagnetic stationary state), the localized SW modes may appear near some (or all) of the SW spectral branches, depending on the structure of the SW spectrum, and on the defect properties.

I. INTRODUCTION

Magnonics—a research field based on the use of spin waves (SWs) (or magnons) as information carriers in magnetic materials for microwave signal processing—is attracting a growing attention of researchers [1–4]. One of the important advantages of SWs for information processing is the excellent possibility to control the SW dispersion law by changing the shape of the used magnetic sample and by varying the direction and magnitude of the magnetic [5] or/and electric bias [6,7] fields applied to this sample. Very interesting results in the SW dispersion control can be achieved when the external bias fields are nonstationary, i.e., are varied substantially on the timescale that is comparable to the time of the SW propagation in the studied sample [5,8]. The control of the SW dispersion can be also effectively achieved in patterned magnetic structures containing layers of different ferromagnetic (FM) materials, or/and in magnetic nanostructures [9–14], that allow one to engineer a desirable form of the SW dispersion [15,16]. Finally, the SW dispersion in a magnetic sample can be varied by reconfiguration of the static magnetization state in a FM sample [17,18]. The last method of dispersion control is convenient to apply in magnonic crystals based on periodic arrays of interacting magnetic elements—nanodots or nanowires. Since the ground state of an isolated FM element of a magnonic crystal at a zero external bias field is, at least, double degenerated, a nanodot array may have several metastable collective states with different SW spectra, different microwave properties, and nontrivial peculiarities in

the SW propagation [19,20]. The collective metastable state of an array can be reconfigured by the application of a short pulse of a bias magnetic field, which opens the way for the creation of magnetic devices for signal processing and microwave applications with microwave properties that can be reconfigured in real time [21–26].

Obviously, any real nanodot array will always contain some defects. The important role of defects in dynamics of usual crystals is well known, see, e.g., a detailed description in Ref. [27]. For our case of artificial magnonic crystals, a rich palette of different defects can be present. These could be the fabrication defects, such as different geometries of the dots, or a deviation of a dot positions from the ideal one, or even the absence of some dots at their intended locations. Another kind of defect in magnonic crystals could appear even in the "atomically ideal" arrays. These defects, that are breaking the ideal periodic static magnetic configuration of an array, could be caused by the reversal of the spatial orientation of the magnetic moments of some dots (or dot clusters) and aligning them in the direction that is opposite to that of the other dots in the array [28–30]. It is also possible to have the formation of the so-called "linear defects," forming a domain wall between the dot clusters having the opposite directions of the dot magnetic moments [31]. Frequently, such linear defects are topologically protected, and they may appear in the course of the array's reconfiguration process, or may be created by the thermal fluctuations [22,23]. Thus, it is important to investigate the influence of various kinds of defects on the dynamic properties of a nanodot array.

It should be noted that the defects in a an array of interacting magnetic dots could find their own unique applications,

*Corresponding author: verrv@ukr.net

such as the case for the defects in photonic crystals [32]. Such applications include: Controllable modification of the local dynamic properties in an array due to the appearance of localized defect modes and due to the scattering of the bulk SW modes on a defect [20,33], appearance of the SW waveguides formed by the line defects [34,35], modification of the phase of a propagating SW using the interaction with defect [35–37], etc. The multistability of the static magnetic states of an array allows one to design magnetic arrays with re-configurable defects (e.g., linear defect waveguides). Finally, the investigation of a ferromagnetic resonance in an array containing defects can give us valuable information about the SW spectra in the array and the interaction between the nanodots forming this array [33].

Previous studies of the SW modes in a nanodot array with defects were limited to the numerical investigations of the localized SW modes created by point defects in a two-dimensional dot array [33], and studies of the magnon modes, localized at an edge of a finite dot array [38–41]. An analytical study of the localized SW modes in a magnetic dot array existing in a ferromagnetic ground state performed in the limit case of "weak" defects was presented in Ref. [42]. A somewhat similar problem of defect modes in a ferromagnetic film within the Heisenberg model was studied in Ref. [43]. The role of a nonideal periodicity on the dynamic properties of "continuous" magnonic crystals and edge magnon states in such crystals was studied in Refs. [44–47].

The aim of our current paper is to present a comprehensive analytical and numerical study of the localized SW modes associated with a single isolated defect in a two-dimensional array of magnetic nanodots coupled by a magnetodipolar interaction. Both conditions for the defect mode localization and the peculiarities of the localized defect mode structure are considered. Two kinds of isolated defects are considered: (i) point defect (a dot with a different eigenfrequency but with the same magnetic moment and, therefore, the unchanged interaction with the other dots), and (ii) the dipolar defect, i.e., the dot having a different magnetic moment and, therefore, the different strengths of the dipolar interaction with the other dots in the array. Any real defect, if not belonging to one of these limiting types, can be considered as a superposition of point and dipolar defects. Note, that our analysis is not limited to the case of an array having a simple lattice existing in a ferromagnetic stable state (the same direction of static magnetization in all the dots of the array), and arrays with a complex static state of the dot static magnetization are also considered. In particular, the antiferromagnetic state of magnetization of a square dot array, which is the true ground state in this geometry at a zero-bias magnetic field [28], is discussed in detail. For such a complex array, it is explained how the interplay between the different SW dispersion branches may affect the formation of the localized SW modes, and what information about the array's SW spectrum can be extracted from the results of the investigation of the SW defect modes in this array.

The article is organized as follows. In Sec. II, an analytical theory formulating the conditions of the SW mode localization and calculating the frequencies of the localized SW defect modes is presented. In Sec. III, a numerical study of the localized SW mode frequency and structure for the case

of an array in a ferromagnetic stable state is presented and compared with the analytical predictions. A complex array existing in the two-sublattice antiferromagnetic ground state is discussed in Sec. IV for the cases of merged and separated SW dispersion branches. Finally, conclusions are presented in Sec. V.

II. THEORY

A. General equations

Let consider a two-dimensional planar array of magnetic nanodots, which are located at the points r_j (radius-vector r_j defines the positions of the dot centers on a plane). We assume that all the dots are in a single-domain saturated state, and their magnetic state is fully described by the magnetization vector $M_j(t)$. In other words, we use a macrospin approximation for the static magnetization of any dot in the array, which is valid for nanodots of a sufficiently small size. The limitations following from this macrospin approach can be released by using the formalism from Ref. [48], but it should be noted, that as soon as the static and dynamic magnetizations of a single dot become spatially nonuniform, the interdot dipolar interaction becomes substantially smaller, and all the collective phenomena in an array will be significantly weakened [49,50]. Since below, we will consider only the linear collective SW excitations in a dot array, it is possible to represent the magnetization of the jth dot as $M_j = M_s(\mu_j + m_j)$, where M_s is the dot saturation magnetization μ_j, $|\mu_j| = 1$ is the unit vector in the direction of dot static magnetization, and m_j ($m_j \perp \mu_j$, $|m_j| \ll 1$) is the dimensionless small deviation of the dot magnetization from its static value. In contrast to the approach of Ref. [42] where the canonical magnon amplitudes (magnon creation/annihilation operators) were used, here, we will work directly with the vectors m_j. This method allows to work directly with the characteristics of a nanodot array without the necessity of the preliminary diagonalization of the Hamiltonian and is more convenient for numerical analysis [20]. According to Ref. [20], the eigenfrequency ω_ν and corresponding profiles $m_{\nu,j}$ of collective SW excitation of an array satisfy the following equation:

$$-i\omega_\nu m_{\nu,j} = \mu_j \times \sum_l \hat{\Omega}_{jl} \cdot m_{\nu,l}, \tag{2.1}$$

where

$$\hat{\Omega}_{jl} = \gamma B_j \delta_{jl} \hat{I} + \gamma \mu_0 M_{s,l} \hat{N}_{jl}, \tag{2.2}$$

$B_j = \mu_j \cdot (B_e - \mu_0 \sum_l M_{s,l} \hat{N}_{jl} \cdot \mu_l)$ is the modulus of the static magnetic field of the jth dot, produced by the external bias field B_e, static demagnetization and anisotropy fields, and stray fields from the other dots. The tensor $\hat{N}_{jl}$ is the mutual demagnetization tensor [51], which describes the magnetodipolar interaction between the dots for $j \neq l$ and self-demagnetization together with the material anisotropy [33] for $j = l$. In a general case of a magnetic dot of an arbitrary geometry, the tensor $\hat{\Omega}_{jl}$ is real and satisfies the following symmetry relation: $V_j M_{s,j} \hat{\Omega}_{jl} = V_l M_{s,l} \hat{\Omega}_{lj}$, where V_j is the volume of the jth dot [52].

Equation (2.1) is general and is valid for an arbitrary array either periodic or nonperiodic. Now, we assume that the array

is periodic and sufficiently large (formally, the number of dots $N_d \to \infty$), so the dot positions can be written as $\boldsymbol{r}_j = n_1 \boldsymbol{a}_1 + n_2 \boldsymbol{a}_2$, where $\boldsymbol{a}_i$'s are the basis vectors of the array lattice, and $n_{1,2}$ are integers. For clarity of the derivation of the main equation, here, we restrict our attention only to the case of an array having a simple Bravais lattice (one dot per a primitive cell) and being in the ferromagnetic static state (static magnetization of all the dots is the same). This assumption will be released below in Sec. II C. SW excitations of a periodic array have the form of the Bloch states $\boldsymbol{m}_k$, characterized by the wave-vector $\boldsymbol{k}$, which lies within the first Brillouin zone of the array lattice, resulting in the following change in Eq. (2.1):

$$\boldsymbol{m}_{\nu,j} \to N_d^{-1/2} \boldsymbol{m}_k e^{i\boldsymbol{k}\cdot\boldsymbol{r}_j}. \qquad (2.3)$$

Then, the dispersion equation and the spatial structure of the collective SW modes in the dot array can be determined from the following equation:

$$-i\omega_k \boldsymbol{m}_k = \boldsymbol{\mu} \times \hat{\boldsymbol{\Omega}}_k \cdot \boldsymbol{m}_k, \qquad (2.4)$$

where

$$\hat{\boldsymbol{\Omega}}_k = \sum_l \hat{\boldsymbol{\Omega}}_{jl} e^{i\boldsymbol{k}\cdot(\boldsymbol{r}_j - \boldsymbol{r}_l)}. \qquad (2.5)$$

The Bloch states are the normal magnon SW modes of an array, so if the dynamic magnetization of dots is expanded in a series over the Bloch states with amplitudes c_k, $\boldsymbol{m}_j = \sum_k (c_k \boldsymbol{m}_k e^{i\boldsymbol{k}\cdot\boldsymbol{r}_j} + \text{c.c.})$, the quadratic part of the array's magnetic energy in terms of c_k assumes the following diagonal form:

$$W^{(2)} = \frac{M_s V_d N_d}{\gamma} \sum_k A_k \omega_k |c_k|^2. \qquad (2.6)$$

Here, $A_k = i(\boldsymbol{m}_k^* \cdot \boldsymbol{\mu} \times \boldsymbol{m}_k)$ is the SW mode normalization constant, appearance of which is related the ellipticity of the magnetization precession in the SW mode [20], V_d is the nanodot volume, and N_d is the number of dots in the array.

Now let us assume that a periodic array contains a defect dot, which has geometrical or/and material parameters that are different from all the other dots in the considered array. For definiteness, we will choose the coordinate of the defect dot as $\boldsymbol{r}_j = 0$. The presence of a defect in the array leads to the change in the matrix $\hat{\boldsymbol{\Omega}}_{jl} \to \hat{\boldsymbol{\Omega}}_{jl}^{(0)} + \Delta\hat{\boldsymbol{\Omega}}_{jl}$. It is clear, that, generally, the presence of a defect can lead to two effects. First, the eigenfrequency of the defect dot and the neighboring dots can be changed due to the static demagnetization and static stray fields of the defect dot. This effect is described by the diagonal terms $\Delta\hat{\boldsymbol{\Omega}}_{jj}$. The second effect is the change in the dynamical interaction between the defect dot and all the other dots, which is described by the off-diagonal terms $\Delta\hat{\boldsymbol{\Omega}}_{j0}$ (describing the influence of defect dot on the jth dot) and $\Delta\hat{\boldsymbol{\Omega}}_{0j}$ (describing the influence of the jth dot on the defect dot). The last term can appear, e.g., if the position of the defect dot differs from the ideal one, or if the defect dot has a different shape. Note that, in many physically important cases, the role of $\Delta\hat{\boldsymbol{\Omega}}_{0j}$ is much less important than the role of $\Delta\hat{\boldsymbol{\Omega}}_{j0}$. For example, the variation of the saturation magnetization of a defect leads to $\Delta\hat{\boldsymbol{\Omega}}_{j0} \neq 0$, but $\Delta\hat{\boldsymbol{\Omega}}_{0j} = 0$ [see Eq. (2.2)]. All the other components of $\hat{\boldsymbol{\Omega}}_{jl}$ remain unchanged because

within the macrospin approximation, the presence of a defect dot cannot modify the dipolar interaction between the other pairs of dots.

The eigenfrequencies and spatial profiles of the collective SW modes of an array containing a defect are described by Eq. (2.1). The set of Bloch states Eq. (2.3) forms a complete orthogonal basis for the collective SW excitation of an array, and we can search the profiles of the SW modes associated with the defect as a sum of these Bloch states with the coefficients ψ_k,

$$\boldsymbol{m}_j = \sum_k \psi_k \boldsymbol{m}_k e^{i\boldsymbol{k}\cdot\boldsymbol{r}_j}. \qquad (2.7)$$

In general, some other terms of the form of $\tilde{\psi}_k \boldsymbol{m}_{-k}^*$ could appear in the expression (2.7), which is analogous to the familiar u-v Bogolyubov transformation. These terms (if present) describe the interaction with "formal conjugated" SW modes having the spatial profiles $\boldsymbol{m}_{-k}^*$ and *negative* eigenfrequencies $-\omega_{-k}$ (see details on the formal conjugated solutions in Refs. [20,48]). Note, however, that these terms are important only if the defect dot has a significantly different anisotropy in the plane perpendicular to the static magnetization (either a shape anisotropy or a material anisotropy), or if the defect dot has a static magnetization, that is noncollinear to that for magnetization of the other dots in the array. Otherwise, these terms can be neglected as is performed below. The numerical calculations, presented below, confirm the validity of this simplification in our case.

Using expansion Eq. (2.7) in Eq. (2.1), multiplying Eq. (2.1) by $e^{-i\boldsymbol{k}'\cdot\boldsymbol{r}_j} \boldsymbol{m}_{k'}^* \cdot \boldsymbol{\mu}\times$, taking the sum over $\boldsymbol{r}_j$, and taking into account the relations $\sum_j e^{i(\boldsymbol{k}-\boldsymbol{k}')\cdot\boldsymbol{r}_j} = N_d \delta_{kk'}$ and $\boldsymbol{m}_k^* \cdot \hat{\boldsymbol{\Omega}}_k \cdot \boldsymbol{m}_k = A_k \omega_k$, one can obtain the following equation for the expansion coefficients ψ_k:

$$(\omega_k - \omega)\psi_k A_k + \frac{1}{N_d}\sum_{k'}(U_{k,k'} + V_{k,k'})\psi_{k'} = 0, \qquad (2.8)$$

where the term,

$$U_{k,k'} = \sum_j \boldsymbol{m}_k^* \cdot \Delta\hat{\boldsymbol{\Omega}}_{jj} \cdot \boldsymbol{m}_{k'} e^{i(\boldsymbol{k}'-\boldsymbol{k})\cdot\boldsymbol{r}_j} \qquad (2.9)$$

describes the changes in the dots eigenfrequencies due to the presence of a defect, whereas the term,

$$V_{k,k'} = \sum_{j\neq 0} \boldsymbol{m}_k^* \cdot (\Delta\hat{\boldsymbol{\Omega}}_{j0} e^{-i\boldsymbol{k}\cdot\boldsymbol{r}_j} + \Delta\hat{\boldsymbol{\Omega}}_{0j} e^{i\boldsymbol{k}'\cdot\boldsymbol{r}_j}) \cdot \boldsymbol{m}_{k'} \qquad (2.10)$$

describes the changes in the dynamical interdot interaction. The solution of Eq. (2.8) yields the same number of the SW normal modes as in the case of an ideal array, but now these modes have *different* properties. The general regulations, here, are the same as for the electron or phonon states in nonideal crystals (see, e.g., Ref. [53]). Most of the modes in a system with a defect (except a few localized modes) have the eigenfrequencies, which lie inside the same frequency bands as for the spectrum of an ideal periodic array (bulk spectrum). In our case, these bulk modes correspond to the propagating magnons, and for a case of a sufficiently weak defect, they can be treated within a perturbation theory (analysis of these modes lies outside the scope of current paper). A few modes

with the frequencies situated outside the bulk SW spectrum correspond to the localized SW modes, associated with the defect, i.e., these are the defect modes. Similar to the states localized inside a potential well in a standard quantum mechanics, the states corresponding to these modes cannot be described using any finite order in the perturbation theory, and one should use the full dynamical equations for the analysis of these modes [54].

B. Point defect of an array in the ferromagnetic state

A general solution of Eq. (2.8) cannot be found analytically. In this section, we consider the simplest case of a point defect—a dot having different eigenfrequency but a nonmodified interdot interaction. In practice, this case corresponds to a dot with different material anisotropy. Mathematically, this case is described by a modification of the term $\hat{\boldsymbol{\Omega}}_{00} \to \hat{\boldsymbol{\Omega}}_{00}^{(0)} + \Delta\hat{\boldsymbol{\Omega}}_{00}$, whereas all the other terms remain unchanged. Thus, in Eq. (2.8) all $V_{k,k'} = 0$ and $U_{k,k'} = \boldsymbol{m}_k^* \cdot \Delta\hat{\boldsymbol{\Omega}}_{00} \cdot \boldsymbol{m}_{k'}$.

For a ferromagnetic static state of an array of identical dots [recall, that in Eq. (2.9) the SW mode profiles for an ideal array are used], one can use the approximation, that the vector structure of the SW modes is almost independent of the SW wave-vector $\boldsymbol{m}_k \notin f(\boldsymbol{k})$. This is related to the fact that the precession ellipticity $\boldsymbol{m}_k$ is mainly determined by the shape and material anisotropy of the dots but not by the $\boldsymbol{k}$-dependent interdot interaction. This approximation fails only near the points of instability of the array's static state. Consequently, we can approximate $U_{k,k'} = U_0$, $A_k = A_0$, that allows one to simplify Eq. (2.8) to

$$(\omega_k - \omega)\psi_k + \frac{U_0}{A_0 N_d} \sum_{k'} c_{k'} = 0. \qquad (2.11)$$

This infinite set of equations for $\psi_{k'}$ has nontrivial solutions if the condition,

$$1 + \sum_k \frac{U_0}{A_0 N_d(\omega_k - \omega)} = 0, \qquad (2.12)$$

similar to the familiar Lifshitz equation [53] is satisfied.

Replacing the summation by integration in the above presented equation, we get the final expression which describes the frequency ω_{loc} of a localized mode in an array existing in a ferromagnetic static state and containing a point defect,

$$1 + \mathcal{U}_0 = 0, \qquad \mathcal{U}_0 = \frac{S_0 U_0}{A_0 (2\pi)^2} \int \frac{d\boldsymbol{k}}{\omega_k - \omega_{\text{loc}}}, \qquad (2.13)$$

where integration goes over the first Brillouin zone of the array lattice and S_0 in the area of the lattice unit cell.

From the equation presented above, it is clear, that in the case $U_0 < 0$ (often called a case of an attractive defect), a localized defect mode can appear only *below* the bulk SW spectrum, whereas in the opposite case of $U_0 > 0$ (a repulsive defect), a localized mode can appear only *above* the bulk SW spectrum (recall, that the SW spectrum of a simple array in a ferromagnetic static state consists of only one branch). It is also clear, that the main features of the localized SW defect mode, at least, for a relatively small defect strength $|U_0|$, are determined by peculiarities of the bulk SW spectrum near its bottom for an attractive defect or near its top for

a repulsive defect. Depending on the array geometry, its magnetic state and external conditions, the SW spectrum near the its top (bottom) can be either smooth parabolic (as in the standard quantum mechanics of usual particles) or linear with a nonanalytic peculiarity of the type of $\omega_k = \omega_{\text{ext}} + C|\boldsymbol{k}|$ (as it is typical for the long-range dipolar interaction). We consider both these cases below.

1. Parabolic SW spectrum

The SW dispersion law in a magnetic dot array having a simple lattice and a ferromagnetic static state has an extremum (minimum or maximum) at one of the symmetric points of the first Brillouin zone of the array lattice. In all the symmetric points except $\Gamma = (0,0)$ the SW dispersion is smooth and parabolic and can be approximated as $\omega_k = \omega_{\text{ext}} \pm D(\boldsymbol{k} - \boldsymbol{k}_{\text{ext}})^2$, where k_{ext} is the position of the extremum. In a general case, the coefficient D depends on the direction of the SW wave-vector k, reflecting the anisotropy of the SW spectrum. Here, for simplicity, we consider the case of an isotropic spectrum, which is realized, e.g., in an array with square or hexagonal lattice. This assumption does not qualitatively affect the behavior of a SW mode localized on a point defect, which will be the same for any anisotropic parabolic spectrum realized for lattices having a lower symmetry.

Using the approximate SW dispersion relation ω_k in Eq. (2.13), one obtains the following expression:

$$\Delta\omega = \omega_{\text{loc}} - \omega_{\text{ext}} = \tilde{\omega} \exp\left[-\frac{4\pi A_0 |D|}{S_0 |U_0|}\right], \qquad (2.14)$$

where the parameter $\tilde{\omega} > 0$ for $U_0 > 0$ and $\tilde{\omega} < 0$ for $U_0 < 0$. This parameter cannot be determined accurately within the approximate model since the parabolic approximation is valid only near the spectrum extremum, whereas integration in Eq. (2.13) goes over the whole spectrum. It is clear, that the appearance of a point defect of any, even a vanishingly small strength leads to the appearance of a localized SW mode, exponentially weakly separated from bulk SW spectrum as is the case in a standard quantum mechanics [54].

2. Nonanalytic spectrum

Due to the long-range character of the dipolar interaction, the SW spectrum at the point Γ ($\boldsymbol{k} = 0$) is nonanalytic: $\omega = \omega_{\text{ext}} + C|\boldsymbol{k}|$. Similarly, as was performed above, we assume that the SW spectrum near the point Γ is isotropic. In contrast to the case of a parabolic SW spectrum, the integral in Eq. (2.13) converges at $\omega_{\text{loc}} = \omega_{\text{ext}}$, meaning that Eq. (2.13) can be satisfied only for a *finite* defect strength U_0. Thus, a localized SW mode in this case can appear only if the defect strength exceeds a certain threshold value of $U_{0,\text{crit}}$,

$$|U_{0,\text{crit}}| = \frac{A_0 (2\pi)^2}{S_0} \left(\int \frac{d\boldsymbol{k}}{\omega_k - \omega_{\text{ext}}}\right)^{-1}. \qquad (2.15)$$

The similar existence of the critical defect strength for a local mode to appear is known for vibration modes in crystal lattices [27]. Close to the threshold value of the defect strength, the dependence of the defect mode frequency on U_0 has a

logarithmic peculiarity at $U_0 \to U_{0,\text{crit}}$,

$$U_0 - U_{0,\text{crit}} \sim (\omega_{\text{loc}} - \omega_{\text{ext}}) \ln \frac{\tilde{\omega}}{\omega_{\text{loc}} - \omega_{\text{ext}}}. \qquad (2.16)$$

C. Point defect of a complex periodic array

In this subsection, we consider a case of a complex dot array for which the primitive cell of the array lattice, accounting for the static magnetic state of the array, contains $P > 1$ dots. This can be an array with a complex geometrical lattice as well as an array with dots, equivalent geometrically, but having a different magnetic state, e.g., an antiferromagnetic state with $P = 2$ magnetic sublattices. It is worth noting that the antiferromagnetic ground state is expected for arrays of magnetic particles coupled by a magnetodipolar interaction in a zero (or a sufficiently small) bias magnetic field (see, e.g., Refs. [28,55]). Similar to the case of all the other complex periodic systems (e.g., crystals having several atoms per a primitive cell), the SW spectrum of a complex array contains P SW branches [20], which can overlap or be separated in the frequency domain (see examples in Sec. IV).

The SW modes in the case of an array, containing P magnetic sublattices and a single defect dot, are described by the same Eq. (2.8). The only difference with the previous case is that the summation should be performed over all the SW wave-vectors $\boldsymbol{k}$ and all the P SW branches. In the determination of the parameters $U_{\boldsymbol{k},\boldsymbol{k}'}$, $V_{\boldsymbol{k},\boldsymbol{k}'}$, Eqs. (2.9) and (2.10), the summation goes over all the dots belonging to all the sublattices in an array with corresponding SW amplitudes $\boldsymbol{m}_{\boldsymbol{k},p}$ in the pth sublattice. Similar to the previous section, we consider, in detail, the case of point defect with the only nonzero term $\Delta\hat{\boldsymbol{\Omega}}_{00} \neq 0$.

In contrast to the case of a simple array, the assumption of the constant SW profiles $\boldsymbol{m}_{\boldsymbol{k}}$ of all the SW modes can be wrong for a complex array. Indeed, whereas the precession ellipticity will be, still, mainly determined by the shape and material anisotropies of the dots, the mutual relation between the oscillation amplitude and phase in different sublattices will be determined only by the interdot dipolar interaction, and, therefore, will significantly depend on the SW wave vector. Also, the mode ellipticity could be different for different SW branches (see example below in Fig. 9).

In order to show qualitatively the main features of the SW spectrum in such a case, we simplify the problem, assuming that the SW structure $\boldsymbol{m}_{\boldsymbol{k}}$ is independent of the SW wave-vector $\boldsymbol{k}$ within each of the SW branches, but it depends on the SW branch number, i.e., $\boldsymbol{m}_{\boldsymbol{k},p} = \boldsymbol{m}_p$, $p = 1, 2, \ldots, P$. Then, the solvability conditions for Eq. (2.8) are simplified to

$$\det[\delta_{pq} + \mathcal{U}_{pq}] = 0, \qquad (2.17)$$

where we introduced a $P \times P$ matrix of the following form:

$$\mathcal{U}_{pq} = \frac{S_0 \boldsymbol{m}_p^* \cdot \Delta\hat{\boldsymbol{\Omega}}_{00} \cdot \boldsymbol{m}_q}{(2\pi)^2 A_p} \int \frac{d\boldsymbol{k}}{\omega_{\boldsymbol{k},p} - \omega_{\text{loc}}} \qquad (2.18)$$

(compare Eq. (2.18) with Eq. (2.13)). In a general case, Eq. (2.17) could have the number of solutions, that is equal to the number of the separate SW branches, i.e., in the case of an attractive (repulsive) point defect, a localized SW mode could appear below (above) every SW spectral band. Thus, if
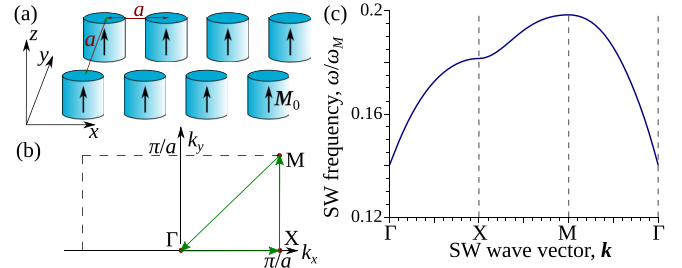

FIG. 1. A sketch of a square array of circular nanodots in the ferromagnetic state (a) and a corresponding SW spectrum (c). Panel (b) shows half of the Brillouin zone of the dot array with symmetric points and the contour $\Gamma \to X \to M \to \Gamma$, used for the plot presented in (c). Calculation parameters are presented in the text.

all the P SW branches are separated, up to P localized SW modes can appear per one defect. However, the number of the localized SW modes could be smaller. Indeed, let us consider the formation of a localized SW mode close to an extremum in a parabolic SW dispersion for the pth SW branch in the case of a vanishingly weak defect. In such a case, only one term $\mathcal{U}_{pp}$, having a peculiarity at $\omega_{\text{loc}} \to \omega_{p,\text{ext}}$, is important. This simplifies Eq. (2.17) to the form

$$1 + \mathcal{U}_{pp} = 0, \qquad (2.19)$$

which is the same as for the case of a simple array lattice. It should be noted, however, that there is one significant difference with the case of a simple lattice: the value of $\mathcal{U}_{pp}$ is proportional not only to the defect strength, but also to the amplitude of the SW mode having wave-vector $\boldsymbol{k}$ that is close to the extremum point of the considered pth SW branch for the corresponding magnetic sublattice, which contains the defect dot. If the bulk SWs near the minimum (maximum) of the pth SW branch has zero amplitude for a particular sublattice, the presence of a weak point defect in this sublattice does not lead to the appearance of a localized SW mode. In general, there could be two possibilities depending on the structure of the SW spectrum: Either a localized mode appears at a defect that is not weak or a localized mode does not appear at all. The realization of both of these cases takes place for a complex array existing in the antiferromagnetic state with two magnetic sublattices (see Sec. IV below).

III. NUMERICAL ANALYSIS OF LOCALIZED DEFECT MODES IN AN ARRAY IN THE FERROMAGNETIC STATE

In this and the following sections, the results of numerical studies of the SW modes, localized on point and dipolar defects, are presented. Here and below, we consider a simple array of circular nanodots, arranged into a square lattice, and having perpendicular-to-plane static magnetization as shown in Fig. 1(a). The following parameters were used in numerical calculations: the dot height-to-radius aspect ratio was $h/R = 5$, the lattice constant $a = 5R$ (absolute value are not specified since, within the macrospin approximation, both self- and mutual demagnetization tensors depend only on the relative sizes [51]), and the crystalline anisotropy was neglected. Note that, for the zero-bias field, the ground state of such a dot array is antiferromagnetic [28], but the static ferromagnetic

state with all the dot magnetic moments parallel to each other could be metastable [29] and easily achieved in practice [18]. In our calculation, we also assumed that external magnetic field is absent. The interdot magnetodipolar interaction was calculated within the point-like-dipole approximation [19]. We do not specify the saturation magnetization and present the results below in dimensionless units ω/ω_M with $\omega_M = \gamma \mu_0 M_s$ for the frequency and $B/(\mu_0 M_s)$ for fields.

The SW spectrum of an ideal periodic dot array in a ferromagnetic static state is shown in Fig. 1(c). The dependence ω_k has a minimum with a nonanalytic peculiarity at the point Γ of the first Brillouin zone ($\mathbf{k} = 0$), and a maximum with the parabolic dispersion at the point M [$\mathbf{k} = (\pm\pi/a, \pm\pi/a)$].

To obtain frequencies and profiles of all the SW modes in a dot array, including the localized defect modes, the eigenproblem Eq. (2.1) was solved numerically for a $N \times N$ nanodot array. In order to avoid the edge effects, periodic boundary conditions were applied. A localized mode in the simulations can be easily identified by its frequency, lying outside the bulk SW spectrum, which was also calculated numerically for the same size of the array and verified by looking at the mode profile. A problem with the identification may appear in the case of small defect strength and, consequently, small separation $\Delta\omega$ of the mode frequency from the bulk spectrum. If this problem appears, we studied how this frequency separation evolves with the size N of the simulated array. If the product $\Delta\omega N$ increases with N, the real localized state is present; otherwise, it is a finite-size numerical artifact. The defect strength for which $\Delta\omega N$ is constant corresponds to the critical defect strength required for a localized mode formation. Array sizes up to 40×40 nanodots were used in the simulations.

A. Point defects

A point defect of an array was simulated as a dot having additional out-of-plane uniaxial anisotropy, characterized by the anisotropy field B_{an}. This anisotropy field leads to the modification of static internal field in the defect dot: $B \rightarrow B + B_{an}$, which contributes to the term $\Delta\hat{\mathbf{\Omega}}_{00}$. Noting that the SW vector structure in the considered square array of circular nanodots is approximately equal to $\mathbf{m_k} \approx (1, i, 0)$, one can find that the strength of the defect is described in Eq. (2.13) by the term $U_0/A_0 = \gamma B_{an}$.

The frequencies of the localized defect mode as functions of the additional defect anisotropy B_{an} are shown in Fig. 2. In accordance with the theoretical prediction for $B_{an} > 0$ (repulsive defect), the local mode appears at vanishingly small defect strength above the bulk SW spectrum, which demonstrates the parabolic behavior near its maximum. For small values of B_{an}, the frequency of the defect mode lies very close to the bulk SW spectrum with exponentially weak separation. In contrast, in the case of negative defect anisotropy $B_{an} < 0$ (attractive defect), the localized mode appears below the SW spectrum only if the defect strength exceeds the threshold value of $|B_{an,th}| \approx 0.034 \mu_0 M_s$, in perfect agreement with Eq. (2.15). In this case, the frequency of the defect mode moves away from the bottom of the bulk spectrum much faster than in the case of positive B_{an}. At a sufficiently large defect strength $|B_{an}|$, the frequency of the localized mode depends
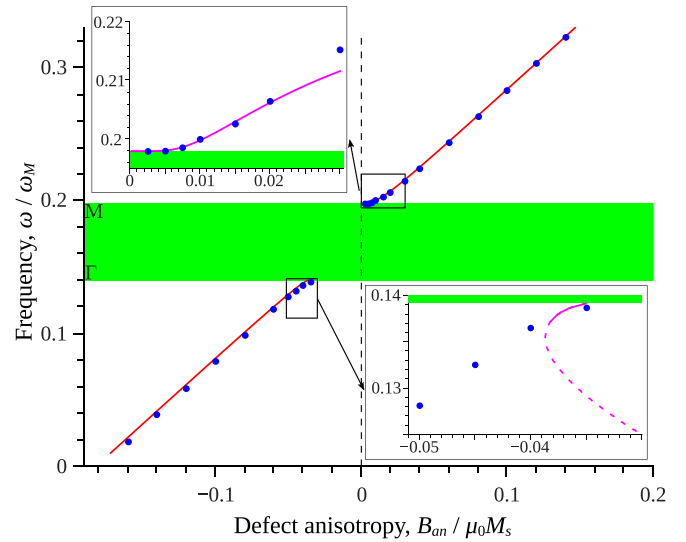

FIG. 2. Dependence of the frequency of a defect mode localized on an anisotropic point defect inside an FM-state array on the magnitude of the additional (defect) anisotropy field B_{an}: (dots) numerical calculations; (lines in the main panel) full Eq. (2.13); (lines in the insets) approximate expressions Eqs. (2.14) and (2.16), respectively. The area shaded in green shows the position of the bulk SW spectrum; symbols M and Γ near the top and bottom of the bulk spectrum denote the symmetric point of the first Brillouin zone at which the spectrum maximum and minimum are reached.

on the defect anisotropy almost linearly. In a general case of a strong defect, the frequency of a localized mode can be estimated as the frequency of an isolated defect dot in a given static field, produced by all the dots in an array. In other words, one can neglect dynamic dipolar interaction between the dots [33]. For the case of an array of circular dots, this approximation yields $\omega_{loc} \approx \gamma(B + B_{an}) + \omega_M N^{(xx)}$, where B is the static field resulting from the external field and static interdot interaction, and $\hat{N}$ is the demagnetization tensor of the defect dot. In all the ranges of defect anisotropy, the frequency of the defect mode is well described by Eq. (2.13) where the numerically calculated bulk SW spectrum (Fig. 2) is used. The approximate expressions Eqs. (2.14) and (2.16) also give correct dependencies of the frequency of the local mode in the cases of small separation from the top or the bottom of the SW spectrum, respectively (see the insets in Fig. 2).

The calculated profiles of the defect modes are shown in Fig. 3 where significant qualitative difference between the modes localized below and above the bulk SW spectrum is clearly seen. As is clear from Eq. (2.11), the bulk SWs close to the spectrum top or bottom contribute mostly to the profile of the defect mode. Consequently, the profile of the defect mode reflects the structure of bulk SWs at the spectrum top or bottom. More rigorously, the spatial profile of the localized mode is described by a localized envelope multiplied by the carrier $\exp[i\mathbf{k}_{ext} \cdot \mathbf{r}_j]$, where $\mathbf{k}_{ext}$ is the point of the minimum or maximum of the bulk SW spectrum, respectively. This property is general and applies for dipolar defects too, see below. In our case, the bottom of the bulk spectrum corresponds to the point $\mathbf{k} = 0$, and the amplitude of the defect mode is simply monotonically decreasing away
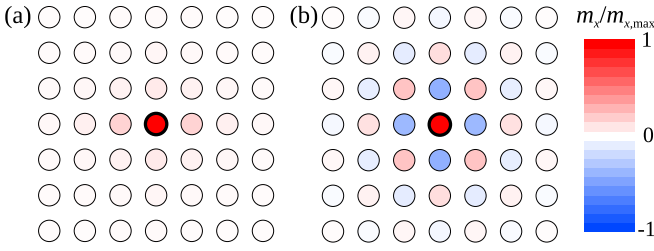
FIG. 3. Profiles of the localized defect modes for a point anisotropic defect: (a) SW mode localized below the bulk spectrum ($B_{an} = -0.05\mu_0 M_s$) and (b) SW mode localized above the SW spectrum ($B_{an} = 0.01\mu_0 M_s$). The defect dot is the central one denoted by the thick edge.

from the defect dot [see Fig. 3(a)]. In contrast, the spectrum maximum is located at $k_M = (\pi/a, \pi/a)$, which creates the carrier $e^{ik_M \cdot r_j} = (-1)^{j_x + j_y}$, so the magnetization in neighboring dots precesses with the π phase shift [see Fig. 3(b)]. Also, the profile of the defect SW mode becomes more localized with the increase in a defect strength.

B. Dipolar defects

A dipolar defect, the dot with modified interdot magnetic dipolar interaction, appears if the defect dot has different geometry and/or saturation magnetization. In a general case, the variation of these parameters leads also to the modification of the dot eigenfrequency. In this subsection, we are considering a specific case when only the interdot interaction with the defect dot is modified, whereas its eigenfrequency remains unchanged. Such a case can be achieved if a defect dot has the same saturation magnetization and shape but different volume. Within the point-like-dipole approximation of the interdot interaction, used here, the tensor $\hat{N}_{j0}$ depends on the volume of the defect dot V_0—it is proportional to the magnetic moment $\mathcal{M} = M_s V_0$ of the defect dot, whereas the tensor $\hat{N}_{0j}$ is completely independent of V_0 so that the static field in the defect dot, created by its neighbors, remains unchanged [outside of the applicability range of the point-like-dipole model, e.g., for dense arrays, a dependence of $N_{0j}(V_0)$ is present, but it is much weaker than the dependence $N_{j0}(V_0)$]. This model allows us to ignore the effects related to the change in the defect dot eigenfrequency and to consider a pure effect of the local modification of the interdot dipolar interaction.

A dipolar defect creates a spatially nonuniform distribution of the static magnetic field in the neighboring dots, field well, or field hill in which defect modes could be localized. The above described point defect also creates a well or hill (in magnetic energy profile), but they are pointlike—only the defect dot lies within the well or hill. In contrast, a dipolar defect creates an extended well or hill with many dots inside it. The calculated frequencies of the localized modes caused by the dipolar defect are shown in Fig. 4. The main difference comparing to the case of the point defect is that the dipolar defect can lead to the appearance of several localized modes, similar to the well-known case of a finite-depth potential well in quantum mechanics [54]. In the case of positive change in the magnetic moment of the defect dot $\Delta\mathcal{M} > 0$, the static internal field in neighboring dots decreases, and the local
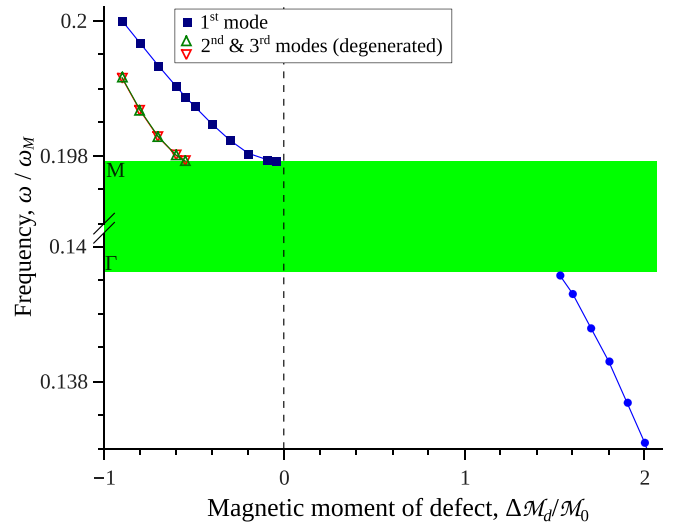

FIG. 4. Dependence of the frequency of a SW mode localized on a dipolar defect inside a FM-state dot array on the defect strength characterized by the relative change in the magnetic moment $\Delta\mathcal{M}/\mathcal{M}_0$ of the defect dot (numerical calculation). The area shaded in green shows the position of the bulk SW spectrum.

modes appear below the bulk SW spectrum. Similar to the situation seen for a point defect, a localized mode appears only at sufficiently large magnitudes of the defect strength $\Delta\mathcal{M}$, which should exceed a certain threshold value. This property is a consequence of a nonanalytic behavior of the SW spectrum at its minimum. The corresponding defect mode has a simple monotonic profile in all the dots except for the defect one [Fig. 5(a)], which reflects the structure of the bulk SWs at the bottom of the spectrum ($k = 0$). At a higher defect strength ($\Delta\mathcal{M}/\mathcal{M}_0 \gtrsim 3$), the higher-order localized defect modes appear, but such a large magnitude of $\Delta\mathcal{M}$ is hard to realize in experiment, and, therefore, the region of so large $\Delta\mathcal{M}$ values is not shown in Fig. 4.

The case of negative $\Delta\mathcal{M}$ is of particular interest because it includes the situations that can be easily realized in practice: An array with one dot having reversed magnetization (which corresponds to $\Delta\mathcal{M} = -2\mathcal{M}_0$) or the absence of one dot
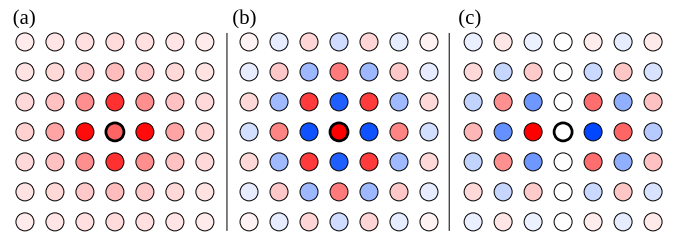

FIG. 5. Profiles of localized defect modes caused by a dipolar defect: (a) localized SW mode appearing below the bulk SW spectrum (for $\Delta\mathcal{M} = 2\mathcal{M}_0$), (b) first (highest in frequency) localized mode appearing above the SW spectrum ($\Delta\mathcal{M} = -0.8\mathcal{M}_0$), (c) frequency-degenerate second and third localized modes appearing above the spectrum ($\Delta\mathcal{M} = -0.8\mathcal{M}_0$) having the same instant profiles but opposite sense of the profile rotation, clockwise and counterclockwise, respectively. The color scale is the same as in Fig. 3; the defect dot is denoted by the thick edge.
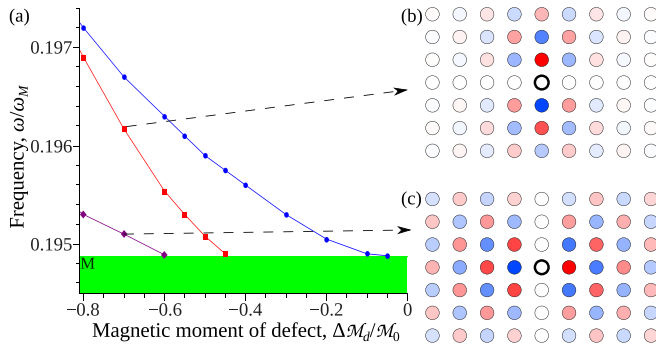
FIG. 6. (a) Frequencies of localized defect SW modes for a dipolar defect in an array having a rectangular lattice. (b) and (c) Profiles of the second (b) and third (c) localized modes for $\Delta\mathcal{M} = -0.7\mathcal{M}_0$. The green area in (a) denotes the position of the bulk SW spectrum; color scale is the same as in Fig. 3.
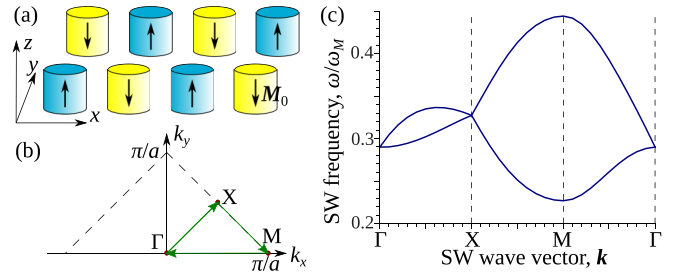

FIG. 7. (a) A sketch of a square array of the circular nanodots array in the CAFM state; (b) half of the magnetic Brillouin zone of an array in the CAFM state demonstrating the symmetric points and the contour $\Gamma \rightarrow X \rightarrow M \rightarrow \Gamma$ in (c) (arrows); (c) bulk SW spectrum of a dot array in the CAFM state at a zero external bias field. Calculation parameters are described in the text.

($\Delta\mathcal{M} = -\mathcal{M}_0$). The defect dot with $\Delta\mathcal{M} < 0$ creates a field hill in the neighboring dots, and the localized modes appear above the bulk SW spectrum. As for the case of the point defect, the first localized mode appears at a vanishingly small defect strength. In contrast, higher-order local modes appear at a finite defect strength. Thus, we can conclude that the behavior of the first local mode in the case of dipolar defect is the same as that of the local mode in the case of the point defect and it reflects the structure of the SW spectrum at its top/bottom in the same manner. Namely, for the parabolic SW spectrum, the first local mode exists at any nonzero defect strength, whereas for the nonanalytic spectrum, the localization happens only at finite defect strength exceeding a certain threshold. The higher-order localized modes in both cases appear at the certain finite strength of the dipolar defect: The stronger the defect is, the more modes appear. A similar feature is also known in quantum mechanics [54].

The profiles of the localized modes above the bulk SW spectrum reflect the fact that the spectrum maximum takes place at $\boldsymbol{k} = (\pi/a, \pi/a)$ and, thus, have the carrier $(-1)^{j_x+j_y}$. The first mode has a zero azimuthal number and a standing profile, shown in Fig. 5(b). The second and third modes in the considered case are degenerated. They have the same instant profile with the nodal line [Fig. 5(c)], but these nodal lines are rotating in the opposite azimuthal direction, clockwise and counterclockwise, respectively. Thus, these are modes having the azimuthal number $n_\phi = 1$. At a larger defect strength, one can expect the formation of higher-order azimuthal local modes.

The frequency degeneracy of the local modes in the studied array is caused by a high in-plane symmetry of array, which results in an isotropic SW spectrum close to its maximum. If this symmetry is broken, the mode degeneracy is lifted. To prove that, we simulated an array of circular nanodots arranged into a rectangular lattice (lattice constants $a_x = 5.5R$, $a_y = 4.5R$). As one can see from Fig. 6, the mode degeneracy is lifted in this case, and two standing modes with nodal lines along either x or y directions appear instead of the above-mentioned rotating azimuthal modes.

Finally, it is worth noting that, in the case of a dipolar defect, the localized modes are located much closer to the

bulk SW spectrum, compared to the case of a point anisotropic defect of the comparable strength ($\Delta\mathcal{M} = \Delta B_{an}V_d/\mu_0$); but a dipolar defect could create several local modes. This feature allows one to discuss the properties of the local modes for a real case of a "combined" defect where both eigenfrequency and dipolar interactions are modified. An important example of this case is the defect dot made with the material having different saturation magnetization. For such a general case, one should expect the formation of one well-separated local mode, associated with the modified eigenfrequency, which can be studied in the approximation of a point defect, and a set much closely located to the bulk spectrum dipolar local modes. Such a case was observed in Ref. [33] for a dot with reversed magnetization. Note, however, that if the modifications of both the eigenfrequency and the magnetic moment of a defect dot are small, only one localized SW mode will be formed, and its behavior will be the same as discussed above.

IV. LOCAL MODES IN COMPLEX ARRAYS: ANTIFERROMAGNETIC STATE OF A SQUARE NANODOT ARRAY

A. Case of merged SW branches (zero-bias field)

The peculiarities of the defect mode formation in a complex magnetic nanodot array are considered, here, on the example of circular nanodot array, arranged into a square lattice, existing in a chessboard antiferromagnetic (CAFM) state, which is the true ground state of such arrays in a zero field (i.e., it corresponds to the global energy minimum) [19,20,28]. A sketch of a CAFM state is shown in Fig. 7(a). An array in the CAFM state has two magnetic sublattices with opposite static magnetizations [shown by different colors in Fig. 7(a)]. Consequently, the bulk SW spectrum consists of two branches with the magnon wave vectors lying inside the magnetic Brillouin zone, i.e., the Brillouin zone for one sublattice, see Fig. 7(b). For the calculations, we use the same nanodot parameters as above ($h/R = 5$) and the reduced lattice constant of $a = 4R$.

Depending on the external magnetic field, the SW branches can overlap or not, creating, thus, one or two SW bands. For any of these branches, both analytical (parabolic) and non-analytical behavior of the dispersion relation can take place
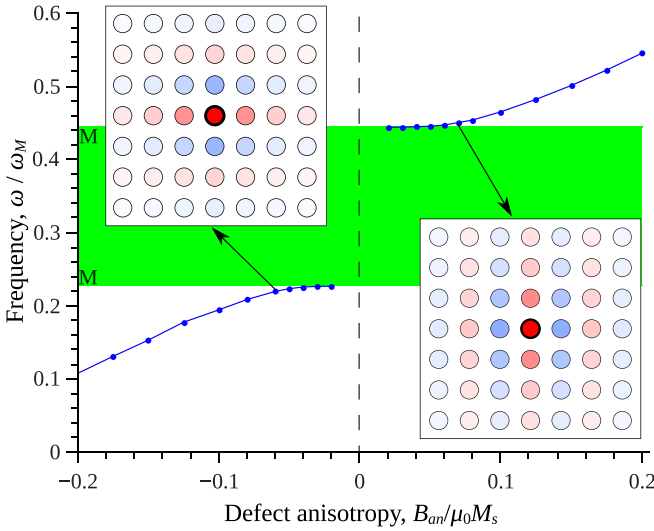
FIG. 8. Dependence of the frequency of the defect SW mode localized on an anisotropic point defect in a dot array existing in the CAFM state in the zero-bias field (numerical calculations). The green-shaded area denotes the position of the bulk SW spectrum. The insets show the profiles of the corresponding localized defect modes. The color scale is the same as in Fig. 3.
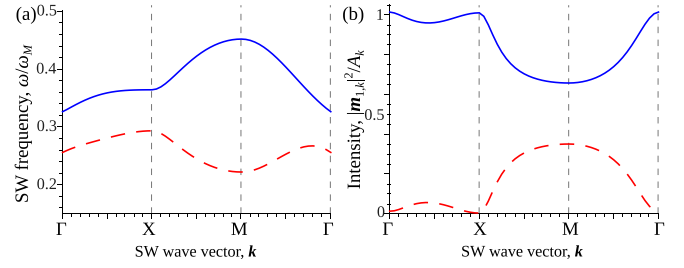

FIG. 9. (a) Bulk SW spectrum of a dot array in a CAFM state for the bias magnetic-field $B_e = 0.035\mu_0 M_s$; (b) Intensity of the magnetization oscillations in the "parallel sublattice" for both upper (solid line) and lower (dashed line) branches of the bulk SW spectrum. For the case of an "antiparallel sublattice," the behavior of the SW amplitudes is reversed: The upper and lower curves in panel (b) describe the SW amplitudes in the lower and upper SW bands, respectively.

near the points of extrema. First, let us discuss the case of overlapping SW branches, which is realized in small external fields, in particular, in the case of the zero external field, considered here. The bulk SW spectrum in this case is shown in Fig. 7(c). Both the minimum and the maximum of the bulk SW spectrum are located at point M of the magnetic Brillouin zone [$k = (0, \pi/a)$ or, equivalently, point $k = (\pi/a, 0)$] (for more information, see Ref. [20]). In this case, the nonanalytical behavior of the magnon spectrum appears to be hidden inside the energy band, and both spectrum minimum and maximum demonstrate a smooth parabolic behavior in their vicinities.

A point defect of an array was simulated in the same manner as in previous section; a dot having additional out-of-plane anisotropy is characterized by the anisotropy field B_{an}. If the external magnetic field is absent, the sublattices of the array are equivalent, that leads to the merging of the branches at symmetrical points [19]. Thus, it does not matter in which particular sublattice the defect dot is located—the properties of the defect mode will be the same. The calculated dependence of the defect mode frequency is shown in Fig. 8. As expected, a localized mode appears at a vanishingly small defect strength, and it is exponentially weakly separated from the bulk spectrum at small B_{an}. It is interesting to note that the localized modes both below and above the bulk SW spectrum have similar profiles (see the insets in Fig. 8). This similarity follows from the fact that both the minimum and the maximum of the bulk SW spectrum are located at the same point M in the first Brillouin zone of the array.

B. Case of a gap between SW branches (non-zero-bias field)

When a sufficiently large bias magnetic-field $\boldsymbol{B}_e = B_z \boldsymbol{e}_z$ is applied to the considered array existing in the CAFM state, the SW branches become separated, and two distinct SW

bands are formed as shown in Fig. 9(a) for the case of $B_z = 0.035\mu_0 M_s$. In this case, the points with the nonanalytical dispersion relation could either correspond to the real extrema (as for the higher band) or be hidden (as for the lower band), see Fig. 9(a). Similar to the previous subsection, we calculate the frequencies of local modes for a point anisotropic defect. At a non-zero-bias field, the sublattices of an array having opposite static magnetization directions are not equivalent anymore. Thus, the behavior of the defect modes depends on which sublattice the defect dot belongs to. We will call the sublattice having static magnetization in the field direction (opposite to the field direction) the parallel sublattice (antiparallel sublattice). Both these cases are analyzed in the following subsection, and the results are presented in Fig. 10.
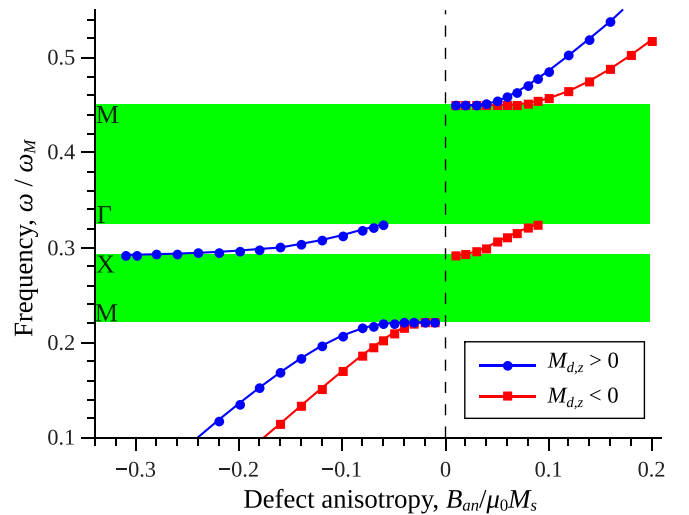

FIG. 10. Dependence of the frequency of the SW mode localized on a point anisotropic defect in an array existing in the CAFM state at $B_e = 0.035\mu_0 M_s$ (numerical calculations) in the case of a defect dot located into the parallel (having static magnetization in the direction of the external bias magnetic-field $M_{d,z} > 0$) and into the antiparallel sublattices (static magnetization opposite to the external field $M_{d,z} < 0$). The green-shaded area denotes the position of the bulk SW spectrum.

1. Defect in the parallel sublattice

First, let us consider the case when the defect dot belongs to the sublattice with the static magnetization parallel to the bias field. In the upper spectrum branch, the bulk SW always have nonvanishing amplitude in the parallel sublattice [Fig. 9(b)]. Thus, according to the theory presented in Sec. II C, a defect dot in this case should lead to the formation of localized SW modes both below and above the upper SW branch. The calculations confirmed this prediction. At a positive defect anisotropy, a localized mode appears for a vanishingly small defect strength above the upper SW branch since the maximum of this branch is parabolic [M point, see Fig. 9(a)]. For a negative defect anisotropy, the localized mode appears at a finite value of B_{an} below the upper SW branch, that reflects nonanalytical spectrum behavior at the branch bottom (the Γ point). With the increase in the defect strength, the frequency of the defect mode slowly approaches the lower SW band and merges with it at $B_{an} \approx -0.31\mu_0 M_s$.

A different situation takes place near the lower SW band. Whereas, in the M point, corresponding to the band minimum, the bulk SWs have a finite amplitude in the parallel sublattice, in the X point (the band maximum), the SW amplitude in the mentioned sublattice is zero. Consequently, the defect mode appears only below the lower SW band for $B_{an} < 0$, whereas no localized mode exists in the spectral gap above the lower band at any defect strength. Thus, there is an asymmetry of the defect mode appearance: Two defect modes are present for an attractive defect and only one for a repulsive defect. This asymmetry reflects the structure of the bulk SWs near the extrema of SW bands and may be used for the identification of the defect location in this or that sublattice.

2. Defect in the antiparallel sublattice

In the case when a defect dot belongs to an antiparallel sublattice, the behavior of the defect modes is similar. The only difference is the fact that the SW amplitudes in the lower bulk SW dispersion branch are nonzero in the antiparallel sublattice. Consequently, localized defect SW modes appear both below and above the lower SW band (see the red squares in Fig. 10). It is interesting to note that, for the case of $B_{an} > 0$, a localized defect SW mode approaches the upper bulk SW band and disappears inside it much faster than in the case of a parallel sublattice. This difference is, evidently, related with the peculiarity of the bulk SW spectrum near its extrema.

Near the upper SW band, one can see the asymmetry of the defect mode formation, similar to the one discussed above for the defect dot in the parallel sublattice: A localized mode appears only above the upper band for positive defect anisotropy. The defect mode is absent for the same reason because the SW amplitude in the antiparallel sublattice at point Γ, which corresponds to the band minimum, is very small (but, strictly speaking, still nonzero). Consequently, the effective defect strength $m_p^* \cdot \Delta\Omega_{00} \cdot m_p$ in Eq. (2.18) is also small, and it is not sufficient to overcome the critical value for the defect formation, which is finite due to nonanalytic peculiarity of the bulk SW spectrum. With an increase in $|B_{an}|$, this threshold value also becomes larger due to the interaction with the lower SW band. Therefore, a localized defect SW mode below the upper bulk SW band is absent at any strength of the attractive defect.

3. Dipolar defects

In the case of dipolar defects in complex dot arrays, one should expect the behavior of the localized defect modes that is qualitatively similar to the one described above for simple dot arrays. Namely, the appearance of the first localized mode at vanishingly small or finite defect strength for the cases of parabolic and nonanalytic bulk SW spectra, respectively, as well the existence of higher-order defect modes at a larger defect strength. Since the dipolar field is long ranged, a dipolar defect dot interacts with all the sublattices. Thus, the properties of the defect SW modes should be much less sensitive to the position of the defect dot in a certain sublattice. However, in the considered case of an array existing in a CAFM ground state, a dipolar defect creates a field well in one sublattice and a field hill in the other sublattice. This counterplay results in a very weak separation of the defect mode frequencies from a bulk SW spectrum for the defects of a reasonable strength, so the observation of the corresponding localized defect SW modes in experiment should be challenging.

V. SUMMARY

In this paper, the conditions of the formation and the basic properties of the SW modes localized on isolated defects in dipolarly coupled arrays of magnetic nanodots were studied. It is shown, that a number and properties of localized defect SW modes depend on whether a particular defect affects the interdot magnetodipolar interaction or not.

In an array with a simple lattice existing in a ferromagnetic static state, the presence of a point defect can lead to the appearance of only one localized defect SW mode. The conditions of the localized mode appearance depend on the peculiarities of the bulk SW spectrum near its minimum or maximum. If the bulk SW spectrum is analytic (with a parabolic dependence on $\boldsymbol{k}$), a vanishingly small defect creates a localized defect mode with exponentially weak separation from the bulk SW spectrum at a small defect strength. In the case of a nonanalytic bulk SW spectrum, a defect mode appears only if the defect strength exceeds a certain threshold value, determined by the whole bulk SW spectrum.

In contrast, a dipolar defect may lead to the appearance of several localized defect SW modes. The conditions of the appearance of the first localized defect SW mode are the same as in the case of a point defect and depend on the peculiarities of the bulk SW spectrum near its minimum or maximum. With an increase in the defect strength, higher localized defect SW modes may appear, and they differ by the azimuthal symmetry. Quantitatively, the gap between the frequencies of these localized SW modes and the bulk SW spectrum is much less than for the SW modes localized on a point defect of a comparable strength.

In a complex array having several distinct bulk SW bands, a point defect may lead to the appearance of localized defect modes near each of the bulk SW bands, and the same conditions, depending on the analytic or nonanalytic properties of the bulk SW spectra near their extrema, govern the

appearance of the localized defect SW modes. Sometimes, however, the number of the localized defect SW modes may become smaller than expected because the amplitude of the bulk SWs on a sublattice containing a point defect may be abnormally small (or even zero) near an extremum of some of the bulk SW bands. In such a case, a localized defect SW mode near this bulk SW band may not appear at all. Moreover, the absence of a localized SW mode may result in the asymmetry of the number of localized SW modes for attractive and repulsive point defects as was discussed above for the case of a square nanodot array in the CAFM ground state. Also, in a complex dot array, a localized SW mode between the bulk SW bands exists only in a certain range of the defect strength. For a sufficiently strong defect, a localized defect mode, created by one bulk SW band, could disappear in the neighboring bulk SW band.

In all these cases, the spatial profile of a localized defect SW mode reflects the structure of bulk SWs in the vicinity of the extrema of the bulk SW spectrum. In particular, at a small defect strength, the profile can be considered as the bulk SW at the spectrum extremum multiplied by a localized envelope, which is simple monotonic in the case of the point defect and more complex in the case of higher-order local modes created by the dipolar defect.

[1] S. Neusser and D. Grundler, Adv. Mater. **21**, 2927 (2009).

[2] V. V. Kruglyak, S. O. Demokritov, and D. Grundler, J. Phys. D: Appl. Phys. **43**, 264001 (2010).

[3] *Magnonics. From Fundamentals to Applications*, edited by S. O. Demokritov and A. N. Slavin (Springer, Berlin, 2013).

[4] A. V. Chumak, V. I. Vasyuchka, A. A. Serga, and B. Hillebrands, Nat. Phys. **11**, 453 (2015).

[5] A. V. Chumak, V. S. Tiberkevich, A. D. Karenowska, A. A. Serga, J. F. Gregg, A. N. Slavin, and B. Hillebrands, Nat. Commun. **1**, 141 (2010).

[6] S.-S. Ha, N.-H. Kim, S. Lee, C.-Y. You, Y. Shiota, T. Maruyama, T. Nozaki, and Y. Suzuki, Appl. Phys. Lett. **96**, 142512 (2010).

[7] F. Matsukura, Y. Tokura, and H. Ohno, Nat. Nanotechnol. **10**, 209 (2015).

[8] A. D. Karenowska, J. F. Gregg, V. S. Tiberkevich, A. N. Slavin, A. V. Chumak, A. A. Serga, and B. Hillebrands, Phys. Rev. Lett. **108**, 015505 (2012).

[9] J. Jorzick, S. O. Demokritov, B. Hillebrands, B. Bartenlian, C. Chappert, D. Decanini, F. Rousseaux, and E. Cambril, Appl. Phys. Lett. **75**, 3859 (1999).

[10] *Spin Wave Confinement*, edited by S. O. Demokritov (Pan Stanford, Singapore, 2009).

[11] S. Tacchi, G. Duerr, J. W. Klos, M. Madami, S. Neusser, G. Gubbiotti, G. Carlotti, M. Krawczyk, and D. Grundler, Phys. Rev. Lett. **109**, 137202 (2012).

[12] S. Tacchi, B. Botters, M. Madami, J. W. Kłos, M. L. Sokolovskyy, M. Krawczyk, G. Gubbiotti, G. Carlotti, A. O. Adeyeye, S. Neusser, and D. Grundler, Phys. Rev. B **86**, 014417 (2012).

[13] X. M. Liu, J. Ding, G. N. Kakazei, and A. O. Adeyeye, Appl. Phys. Lett. **103**, 062401 (2013).

[14] G. N. Kakazei, X. M. Liu, J. Ding, V. O. Golub, O. Y. Salyuk, R. V. Verba, S. A. Bunyaev, and A. O. Adeyeye, Appl. Phys. Lett. **107**, 232402 (2015).

[15] Z. K. Wang, V. L. Zhang, H. S. Lim, S. C. Ng, M. H. Kuok, S. Jain, and A. O. Adeyeye, ACS Nano **4**, 643 (2010).

[16] J. W. Kłos, D. Kumar, M. Krawczyk, and A. Barman, Sci. Rep. **3**, 2444 (2013).

[17] J. Topp, D. Heitmann, M. P. Kostylev, and D. Grundler, Phys. Rev. Lett. **104**, 207205 (2010).

[18] R. Verba, G. Melkov, V. Tiberkevich, and A. Slavin, Appl. Phys. Lett. **100**, 192412 (2012).

[19] P. V. Bondarenko, A. Y. Galkin, B. A. Ivanov, and C. E. Zaspel, Phys. Rev. B **81**, 224415 (2010).

[20] R. Verba, G. Melkov, V. Tiberkevich, and A. Slavin, Phys. Rev. B **85**, 014427 (2012).

[21] S. Tacchi, M. Madami, G. Gubbiotti, G. Carlotti, S. Goolaup, A. O. Adeyeye, N. Singh, and M. P. Kostylev, Phys. Rev. B **82**, 184408 (2010).

[22] J. Ding, M. Kostylev, and A. O. Adeyeye, Phys. Rev. Lett. **107**, 047205 (2011).

[23] R. Verba, V. Tiberkevich, K. Guslienko, G. Melkov, and A. Slavin, Phys. Rev. B **87**, 134419 (2013).

[24] M. Krawczyk and D. Grundler, J. Phys.: Condens. Matter **26**, 123202 (2014).

[25] I. Lisenkov, V. Tyberkevych, L. Levin-Pompetzki, E. Bankowski, T. Meitzler, S. Nikitov, and A. Slavin, Phys. Rev. Appl. **5**, 064005 (2016).

[26] A. Lara, M. J. Robledo, K. Y. Guslienko, and F. G. Aliev, Sci. Rep. **7**, 5597 (2017).

[27] A. M. Kosevich, *The Crystal Lattice: Phonons, Solitons, Dislocations, Superlattices*, second revised and updated ed. (Wiley-VCH Verlag, Weinhein, Germany, 2005).

[28] J. E. L. Bishop, A. Y. Galkin, and B. A. Ivanov, Phys. Rev. B **65**, 174403 (2002).

[29] A. Y. Galkin, B. A. Ivanov, and A. Y. Merkulov, J. Exp. Theor. Phys. **101**, 1106 (2005).

[30] P. V. Bondarenko, A. Y. Galkin, and B. A. Ivanov, J. Exp. Theor. Phys. **112**, 986 (2011).

[31] B. A. Ivanov and V. E. Kireev, JETP Lett. **90**, 750 (2010).

[32] K. Sakoda, *Optical Properties of Photonic Crystals* (Springer, Berlin, 2001).

[33] R. Verba, V. Tiberkevich, E. Bankowski, T. Meitzler, G. Melkov, and A. Slavin, IEEE Magn. Lett. **4**, 4000404 (2013).

[34] I. Lisenkov, S. Louis, S. A. Nikitov, V. Tyberkevych, and A. Slavin, *2015 IEEE International Magnetics Conference (INTERMAG, Beijing)* (IEEE, 2015), pp. 1–1.

[35] S. Louis, I. Lisenkov, S. Nikitov, V. Tyberkevych, and A. Slavin, AIP Adv. **6**, 065103 (2016).

[36] O. V. Dobrovolskiy, R. Sachser, S. A. Bunyaev, D. Navas, V. M. Bevz, M. Zelent, W. Śmigaj, J. Rychły, M. Krawczyk, R. V. Vovk, M. Huth, and G. N. Kakazei, ACS Appl. Mater. Interfaces **11**, 17654 (2019).

[37] K. Baumgaertl, S. Watanabe, and D. Grundler, Appl. Phys. Lett. **112**, 142405 (2018).

[38] I. Lisenkov, V. Tyberkevych, A. Slavin, P. Bondarenko, B. A. Ivanov, E. Bankowski, T. Meitzler, and S. Nikitov, Phys. Rev. B **90**, 104417 (2014).

[39] P. V. Bondarenko, Tech. Phys. Lett. **40**, 813 (2014).

[40] I. Lisenkov, V. Tyberkevych, S. Nikitov, and A. Slavin, Phys. Rev. B **93**, 214441 (2016).

[41] S. Osokin, A. Safin, Y. Barabanenkov, and S. Nikitov, J. Magn. Magn. Mater. **465**, 519 (2018).

[42] E. G. Galkina and B. A. Ivanov, JETP Lett. **104**, 32 (2016).

[43] N.-N. Chen and M. Cottam, Solid State Commun. **84**, 379 (1992).

[44] V. V. Kruglyak, M. L. Sokolovskii, V. S. Tkachenko, and A. N. Kuchko, J. Appl. Phys. **99**, 08C906 (2006).

[45] J. W. Kłos and V. S. Tkachenko, J. Appl. Phys. **113**, 133907 (2013).

[46] R. A. Gallardo, T. Schneider, A. Roldán-Molina, M. Langer, A. S. Núñez, K. Lenz, J. Lindner, and P. Landeros, Phys. Rev. B **97**, 174404 (2018).

[47] J. Rychły and J. W. Kłos, J. Phys. D: Appl. Phys. **50**, 164004 (2017).

[48] R. V. Verba, Ukr. J. Phys. **58**, 758 (2013).

[49] A. Y. Galkin, B. A. Ivanov, and C. E. Zaspel, Phys. Rev. B **74**, 144419 (2006).

[50] A. A. Awad, G. R. Aranda, D. Dieleman, K. Y. Guslienko, G. N. Kakazei, B. A. Ivanov, and F. G. Aliev, Appl. Phys. Lett. **97**, 132501 (2010).

[51] M. Beleggia, S. Tandon, Y. Zhu, and M. De Graef, J. Magn. Magn. Matter. **278**, 270 (2004).

[52] R. Verba, E. Bankowski, T. Meitzler, V. Tiberkevich, and A. Slavin, SPIN **06**, 1640013 (2016).

[53] I. M. Lifshitz and S. I. Pekar, Usp. Fiz. Nauk. **56**, 531 (1955).

[54] L. D. Landau and E. M. Lifshitz, *Quantum Mechanics*, Course of Theoretical Physics Vol. 3 (Pergamon, Oxford, 1965).

[55] K. Y. Guslienko, Appl. Phys. Lett. **75**, 394 (1999).